Chemical Engineering Journal 453 (2023) 139801

Contents lists available at ScienceDirect

Chemical Engineering Journal

journal homepage: www.elsevier.com/locate/cej

SnO_2/ATP catalyst enabling energy-efficient and green amine-based CO_2 capture

Zhan Tan [a], Shangshang Zhang [a], Fangfang Zhao [a,c], Rui Zhang [a,b,c,d], Feiying Tang [a], Kuiyi You [a,c,d,*], He'an Luo [a,c,d], Xiaowen Zhang [a,b,c,d,e,*]

[a] School of Chemical Engineering, Xiangtan University, Xiangtan 411105, PR China
[b] Foshan Green Intelligent Manufacturing Research Institute of Xiangtan University, Foshan 528311, PR China
[c] National & Local United Engineering Research Center for Chemical Process Simulation and Intensification, Xiangtan University, Xiangtan 411105, PR China
[d] Engineering Research Center for Low-Carbon Chemical Processes and Resource Utilizations of Hunan Province, Xiangtan University, Xiangtan 411105, PR China
[e] Key Laboratory of Low-grade Energy Utilization Technologies and Systems (Chongqing University), Ministry of Education of China, Chongqing University, Chongqing 400044, China

ARTICLE INFO

Keywords:
CO_2 capture
Catalytic CO_2 desorption
Heat duty reduction
SnO_2 modified attapulgite
Sold acid catalyst

ABSTRACT

CO_2 capture using aqueous amine solutions necessitates intensive heat duty because the temperature of solvent regeneration required to decompose the carbamate is>120 °C. In this work, we reported a SnO_2 modified attapulgite (SnO_2/ATP) solid acid catalyst to accelerate CO_2 desorption in a rich 5 M monoethanolamine (MEA) solution at 88 °C. The SnO_2/ATP catalyst with improved Brønsted acid sites and strong acid sites worked better than SnO_2 and ATP. Particularly, utilizing 1/2-SnO_2/ATP increased the CO_2 desorption rate and desorbed CO_2 by 265 and 222 %, respectively, as compared to CO_2 desorption without a catalyst. The relative heat duty could be reduced by about 52 % by using 1/2-SnO_2/ATP to regenerate the rich MEA solution, and its catalytic performance was superior to most reported solid catalysts for this purpose. FT-IR technique was employed to confirm the catalytic effect and a possible catalytic CO_2 desorption mechanism was suggested. Additionally, 12 CO_2 absorption–desorption cyclic tests were conducted to certificate the recyclability of 1/2-SnO_2/ATP. These findings demonstrated that SnO_2/ATP catalyst had significant potential for industrial use in low-energy and green amine-based CO_2 capture processes. This study provides a practical strategy for utilizing efficient, affordable and environmentally benign solid acid catalysts for CO_2 desorption, thereby advancing energy-efficient CO_2 capture technology.

1. Introduction

Excess carbon dioxide (CO_2) emission is considered as the main contributor to global warming [1,2]. A variety of technologies have been reported to capture CO_2. Currently, the chemical absorption process using aqueous amine solutions is generally regarded as the most efficient and leading technique for capturing CO_2 from flue gas [2–4]. Nevertheless, the high heat duty of rich absorbent regeneration for CO_2 desorption is the biggest obstacle to the industrial application of this technology [5–7]. Traditional thermal regeneration of CO_2-loaded solvents is achieved by heating the solvents to a higher temperature above 120 °C [2,8,9]. Accordingly, the decrease of solvent regeneration temperature (below 100 °C) while increase of the CO_2 desorption kinetics, and therefore reducing heat duty is the top priority for further advancing the CO_2 scrubbing technology of amine solution.

Considerable efforts have been made for reducing the energy demanded of CO_2 desorption, including process intensification [10], solvent enhancement [6,11] and the addition of additives (carbonic anhydrases [12], metal ions [13], weak acids [14], nanoparticles [15,16]). The catalytic amine solvent regeneration has recently been reported as a promising method to significantly improve the CO_2 desorption rate and lower the energy consumption for the rich amine solution regeneration process. The prominent feature of catalytic CO_2 desorption is that it has the ability to decrease the CO_2 desorption temperature to lower than 100 °C, and thus open the road for the utilization of low-grade heat resources (i.e., industrial waste heat), as a green method for CO_2 desorption.

Various solid acid materials have been utilized to catalyze CO_2

* Corresponding authors.
E-mail addresses: youkuiyi@126.com (K. You), xzhang1@xtu.edu.cn (X. Zhang).

https://doi.org/10.1016/j.cej.2022.139801
Received 7 August 2022; Received in revised form 21 September 2022; Accepted 11 October 2022
Available online 17 October 2022

desorption in the benchmark solvent, monoethanolamine (MEA) solution, and have been proven to be effective in minimizing regeneration heat duty [11,17–21]. Zhang et al. evidenced that zeolite, sulfated metal oxide, and zeolite-supported (sulfated) metal oxide catalysts including, SAPO-34, $SO_4^{2-}/ZrO_2/Al_2O_3$, Fe_2O_3/MCM-41, and $SO_4^{2-}/ZrO_2/Fe_2O_3$/MCM-41 lowered the energy consumption by about 20–40 % [22–25]. According to Sun et al., the NiO/HZSM-5 catalyst enhanced the desorbed CO_2 by 36 % while reducing the energy requirement by 27 % [26]. Xing et al. investigated the use of SO_4^{2-}/ZrO_2-HZSM-5 catalyst in CO_2 desorption, revealing that about 31 % reduction of energy penalty was achieved [27]. Covalent organic frameworks (COFs) and metal–organic frameworks (MOFs) and their derivatives, including Fe_3O_4@UiO-66-SO_4 [20], SO_4^{2-}/ZIF-67-C@TiO_2 [19], Ni/Fe@COF [28], and CeO_2-MOF-HPW [29] were also employed for CO_2 desorption. The results indicated that the heat duty could be reduced by up to 58 %. Baek et al. [30,31] have also verified this to be true by conducting similar catalytic CO_2 desorption tests using the metal oxides as catalysts. However, this solid catalyst-assisted method is in its infant stages and further advancement is still strong required.

Attapulgite (ATP) is a typical phyllosilicate mineral with nanoscale structure, which is widely used in industrial processes as catalyst or catalyst support [32]. The general theoretical chemical formula of ATP is $Al_2Mg_2Si_8O_{20}(OH)_2(OH_2)_4{\cdot}4H_2O$. Two bands of SiO_4 tetrahedra connected by metal ions in octahedral coordination make up the crystal structure of ATP [33,34]. China has significant ATP reserves and accounts for 60 % [35]. ATP is particularly attractive because of its ecological safety,low-cost, large surface area and high stability [36]. Moreover, because of the presence of some cations (Si, Fe, Mg, and Al), hydroxyl and water molecules in the layered structure, ATP possesses both Brønsted and Lewis acid sites (B and L acids) [32]. In particular, the price of ATP is only 10–20 % of the commonly used chemical Si/Al raw materials [33,37]. Accordingly, ATP acts as an appealing solid acid catalyst or catalyst support for various acid catalytic reactions [37]. Additionally, our previous work demonstrated that compared with bentonite and sepiolite clay catalysts, ATP exhibited the best activity in catalyzing the regeneration process of CO_2-loaded monoethanolamine (MEA) solution [38].

Despite this, the catalytic performance of ATP for CO_2 desorption is limited by the low acid sites. Based on the literature, metal oxide modified ATP can improve the catalytic performance by increasing the active site of the catalyst. ATP has unique properties as a catalyst carrier, including increasing metal-carrier interactions, improving metal dispersion, and altering reaction routes during reaction process [39–41]. For example, Wang et al. [42] reported ATP supported nickel catalyst for steam reforming of ethylene glycol. Because of the large metal particle sizes and high surface acidity, the supported catalyst presented a higher catalytic activity. Furthermore, our previous works [17,22] demonstrated that the metal oxides promoted molecular sieve catalysts Al_2O_3/HZSM-5 and Fe_2O_3/MCM-41 could further improve the kinetics of CO_2 desorption for rich MEA solution than the parent molecular sieve. Thus, metal oxide modified ATP catalyst may offer a significant opportunity to further improve the CO_2 desorption rate and decrease the regeneration energy requirement.

However, it is still unknown how ATP as a support behaves and affects the catalytic behavior of active metals in the regeneration process of amine solution. It is generally accepted that the catalyst support not only plays the role of supporting and dispersing active sites, but also may participate in catalytic reaction. On the other hand, SnO_2 is a significant metal oxide because of its advantageous structural, textural, and acidic properties [43,44]. In particular, SnO_2 has a higher strong acid site than that of sn-Beta, ZrO_2 and TiO_2 [45]. Therefore, the synergistic effect of ATP support and SnO_2 is expected to result in remarkable increase in acidic properties, hence enhancing CO_2 desorption in low temperature.

Herein, for the first time, the rich MEA solution regeneration process was catalyzed using the SnO_2 modified ATP catalyst (SnO_2/ATP) to improve the CO_2 desorption kinetics and reduce the energy requirement. For comparison, the catalytic CO_2 desorption activities of ATP and SnO_2 were also studied. The physicochemical characteristics of the catalysts were determined using various characterization techniques, and the structure–property relationship of the catalysts was also correlated. The catalytic impact of the catalyst on solvent regeneration was confirmed using FT-IR technique. The catalyst stability was investigated through twelve cyclic tests, and a potential catalytic mechanism for the CO_2-loaded MEA solution regeneration was proposed. This work may open the way for developing low-cost catalytic materials with desirable physicochemical properties for low-temperature CO_2 desorption, and advancing a significant step towards the establishment of green and low-energy consumption CO_2 capture technology.

2. Experimental

2.1. Chemicals

The chemicals adopted in the present work are presented in supporting information (SI) Section 1.1.

2.2. Catalyst synthesis

The SnO_2/ATP catalyst was synthesized using a precipitation-impregnation method, and the detailed information are supplied in SI Section 1.2. The catalysts with the $SnCl_2{\cdot}6H_2O$/ATP weight ratio of 1/2 and 1/4 were marked as 1/2-SnO_2/ATP and 1/4-SnO_2/ATP.

2.3. Catalyst characterization

The catalyst was characterized using X-ray diffraction (XRD), Fourier transform infrared spectroscopy (FT-IR), N_2 adsorption–desorption experiment, pyridine-adsorption infrared spectroscopy (Py-IR), and temperature programed desorption of ammonia (NH_3-TPD). The detailed information about these characterizations are provided in SI Section 1.3.

2.4. Catalyst test

The experimental setup for catalytic CO_2 desorption in the rich MEA solution is shown in Fig. S1(b), and the details about this device and operating procedures can be found in SI Section 1.4. Three parameters including, CO_2 desorption rate (r_d, mol/s), amount of desorbed CO_2 (n_d, mol), and relative regeneration heat duty (h_r, %) are adopted to evaluate the catalytic performance of the catalysts, and their calculation methods are provided in SI Section 1.4.

3. Results and discussion

3.1. Reliability of the experimental results

The quality of desorbed CO_2 was determined using the gas phase method (n_{dg}) and the liquid phase method (n_{dl}), and the n_{dg} and n_{dl} were then utilized to validate the accuracy of the experimental results. The CO_2 desorption tests without a catalyst (blank test) were conducted three times, and the corresponding amounts of desorbed CO_2, n_{dg} and n_{dl}, were obtained using the two methods, and their absolute relative deviations (ARD) were also calculated. The results are displayed in Figure S3 and Table S1. The repeatability of the three curves is high, indicating the fine stability of the device (Figure S3). The average ARD, which can be derived from Table S1, is 7 %, implying both measurements are accurate.

3.2. Catalytic performance

The CO_2 desorption results in CO_2-loaded MEA solution with four SnO_2 modified ATP (1/2-SnO_2/ATP, 1/3-SnO_2/ATP, 1/4-SnO_2/ATP and

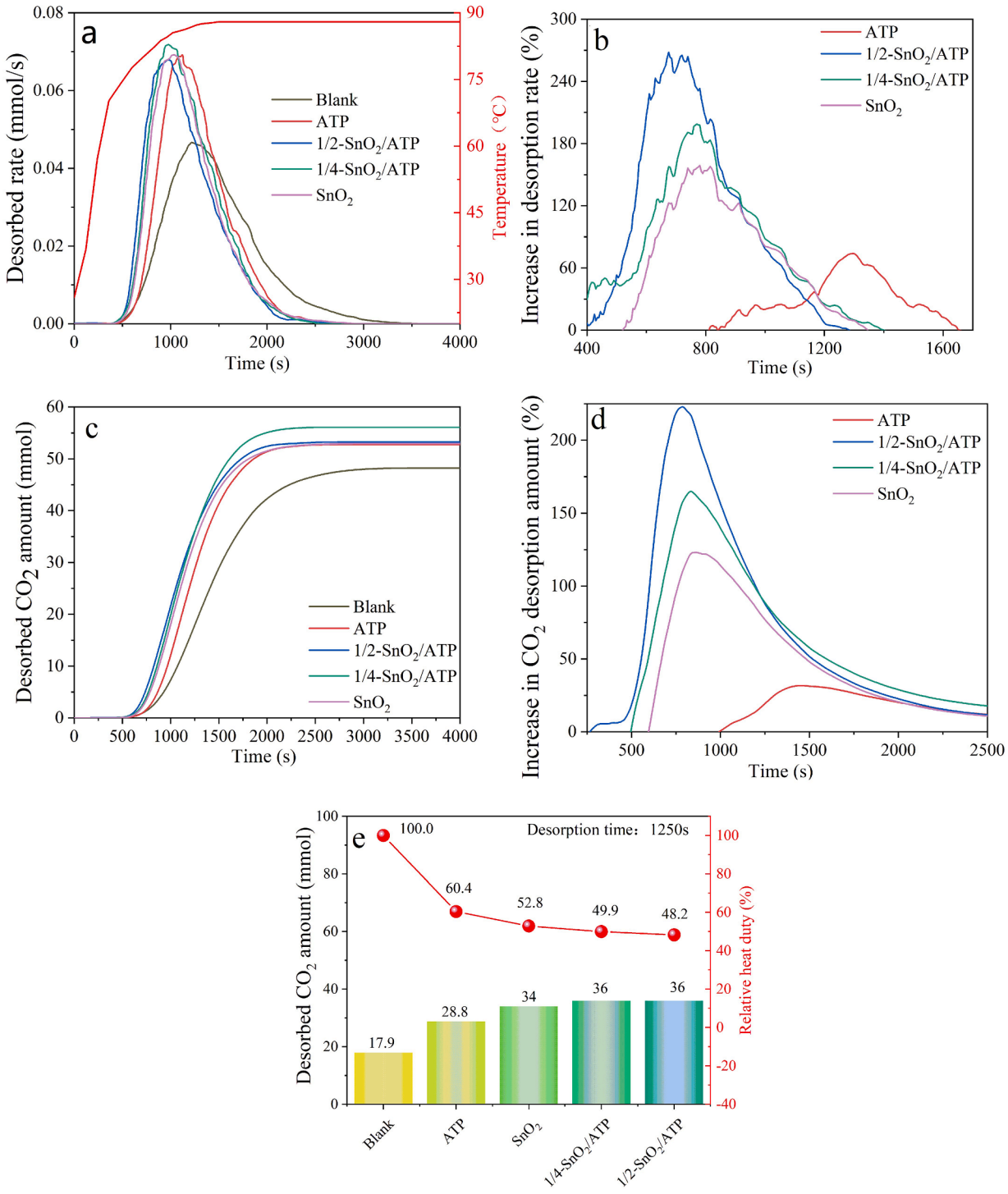

Fig. 1. Effect of catalysts on CO_2 desorption performance. (a) CO_2 desorption rate. (b) Percentage increase in CO_2 desorption rate. (c) Amount of desorbed CO_2. (d) Percentage increase in amount of CO_2 desorption. (e) Amount of CO_2 desorbed and relative heat duty at 1250 s. Desorption conditions, solution: 200 mL 5 M rich MEA solution with the initial CO_2 loading of 0.515 (±0.01) mol CO_2/mol amine, desorption temperature: 25–88 °C, catalyst dosage: 2.5 g (1.25 wt%), flow rate of N_2: 500 mL/min, desorption time: 4000 s.

1/5-SnO_2/ATP), SnO_2 and ATP catalysts, and without a catalyst are presented in Figure S4. All the catalysts accelerated the desorption of CO_2, with 1/2-SnO_2/ATP exhibiting the greatest catalytic performance. However, different metal oxide contents have no significant effect on the catalytic activity. Therefore, two SnO_2 modified ATP (1/2-SnO_2/ATP and 1/4-SnO_2/ATP), SnO_2 and ATP catalysts were selected for further study on their catalytic performance and structure–activity relationship, and the results are displayed in Fig. 1. 1/2-SnO_2/ATP shows the highest catalytic activity, followed by 1/4-SnO_2/ATP and SnO_2, and ATP has the lowest catalytic activity. As illustrated in Fig. 1(a), the CO_2 desorption rate for the blank run achieves its maximum value at 1250 s. All other catalysts peaked earlier than the blank test. Therefore, the first 1250 s of the blank run period was employed as a baseline to assess the catalytic performances of the catalysts.

Fig. 1(a) shows that utilizing 1/2-SnO_2/ATP raised the absolute CO_2 desorption rate by 98 % at 990 s in comparison to the blank test. In addition, compared to the blank run, using 1/2-SnO_2/ATP required 260 s less time (1250–990 s) to achieve the top of its desorption rate. Similarly, the desorption temperature that corresponded to the peak desorption rate of 1/2-SnO_2/ATP was decreased by 2–3 °C. According to Fig. 1(b), due to the introduction of 1/2-SnO_2/ATP, the percentage improvement of the CO_2 desorption rate could reach up to 265 % at 671 s. However, ATP only increased the instantaneous desorption rate by 74.2 % at 1300 s.

Fig. 1(c), (d) depicts the effect of the catalysts on the amount of desorbed CO_2 during the desorption process. It is noted that the blank test released 18.1 mmol CO_2 at 1250 s, but the amount of desorbed CO_2 greatly increased to 36.1 mmol (99 % improvement), when 1/2-SnO_2/ATP was used. When the desorption time was moved forward to 780 s, the addition of 1/2-SnO_2/ATP increased the desorbed CO_2 by 222 % (Fig. 1(d)). Whereas, when ATP catalyst was employed, the maximum percentage in desorbed CO_2 was only 32.2 % at 1420 s. These findings undoubtedly proved that SnO_2 modification of ATP greatly improved its catalytic CO_2 desorption performance in the rich MEA solution

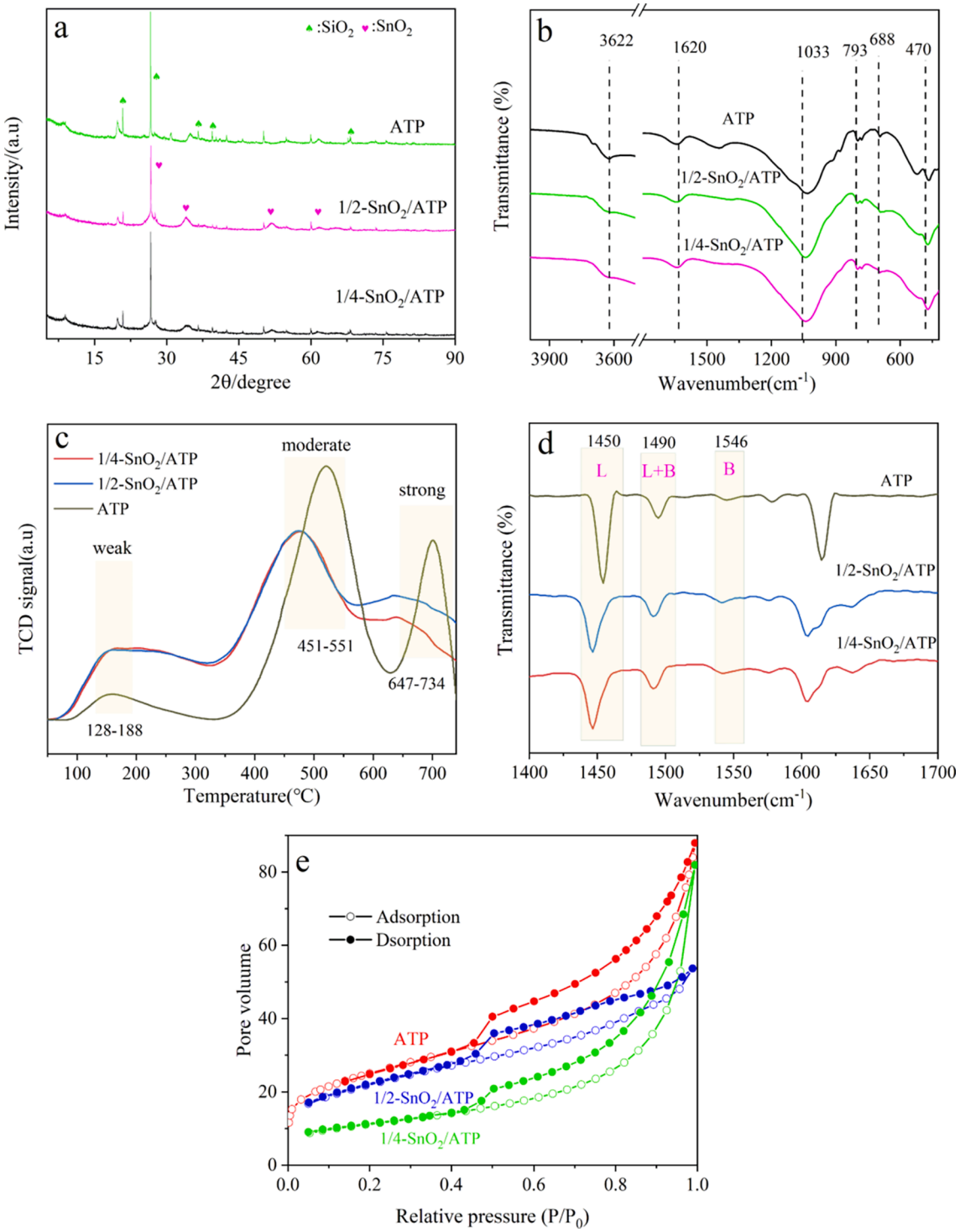

Fig. 2. Characterization results of catalysts. (a) XRD. (b) FT-IR. (c) NH_3-TPD. (d) Py-IR. (e) N_2 adsorption–desorption isotherms.

regeneration process. The introduction of SnO_2/ATP not only considerably increased the CO_2 desorption rate and amount of desorbed CO_2, but also shifted CO_2 desorption to the low temperature region.

The relative heat duty and the amount of desorbed CO_2 during the first 1250 s for the rich MEA solution regeneration process with and without catalysts are given in Fig. 1(e) and S5. The CO_2 desorption experiments were conducted utilizing a simplified batch method without insulators and heat radiation, which resulted in the regeneration heat duty obtained in this study is larger than its true value. At 1250 s, the use of 1/2-SnO_2/ATP increased the desorbed CO_2 by 101 %, while ATP increased by only 60.9 %. Using the non-catalytic desorption process as a baseline, these four catalysts demonstrated the potential to reduce the energy consumption for solvent regeneration. The relative heat duty (%) of the four catalysts was ranked as: 1/2-SnO_2/ATP (48.2) < 1/4-SnO_2/ATP (49.9) < SnO_2 (52.8) < ATP (60.4) < blank run (100). In particular, the addition of 1/2-SnO_2/ATP catalyst could considerably lower the energy consumption by approximately 52 %. The change trend of relative heat duty with desorption time is consistent with the relative heat duty order of 1250 s (Figure S5). On the basis of these findings, it can be concluded that the use of SnO_2/ATP catalyst can greatly accelerates the rate of CO_2 desorption and speeds up the CO_2 release, therefore decreasing the heat duty for CO_2 desorption in rich amine solutions even at low temperatures.

The performance comparison results of the prepared catalysts used in this study and the solid acid catalysts previously reported for the rich MEA solution regeneration process are shown in Table S2. Most reported solid acid catalysts are found to minimize the relative heat duty for the rich MEA solution regeneration process to 60–70 %. In contrast, the relative heat duty was reduced to 48.2 % when 1/2-SnO2/ATP was employed. This suggests that SnO_2/ATP holds considerable promise for lowering energy consumption during rich amine solution regeneration. Furthermore, compared to other reported solid catalysts such as, zeolite molecular sieves, and metal–organic frameworks (MOFs), the cost of ATP (~$23/kg) is probably the cheapest. As a result, due to its ease manufacture, high efficiency, low cost, and environmental friendliness, the SnO_2/ATP catalyst shows significant potential for industrial use in low-energy and green amine-based CO_2 capture technologies.

3.3. Results of catalyst characterization

Fig. 2(a) illustrates the XRD patterns of ATP, 1/4-SnO_2/ATP and 1/2-SnO_2/ATP. The two SnO_2/ATP catalysts exhibit characteristic peaks of ATP, proving that the modification process did not destroy the characteristic structure of ATP. The peaks located at 20.9, 26.5, 36.5, 39.5, 50.1, 60.1 and 68.1° were attributed to the SiO_2 phase in the ATP (PDF#86–2237) [46]. The extra diffraction peaks at 34.1, 51.9, 61.7° were observed for the SnO_2/ATP catalysts, which are the typical characteristic peaks for the SnO_2 phase (PDF#99–0024)[47]. This result indicates that the SnO_2 particles were well dispersed on the surface of ATP or entered ATP channels.

The FT-IR spectra of the three catalysts are depicted in Fig. 2(b). The peak at 3622 cm^{-1} was assigned to the stretching vibration of Al-OH-Al. The O—H bending vibration in physically adsorbed water was responsible for the peak at 1620 cm^{-1} [46]. The peaks at 1033 and 792 cm^{-1} might be associated with the stretch vibrations of M−O−M groups (M = Si, Sn) [48]. The bands at 618 and 470 cm^{-1} are due to the bending vibrations of Si-O [37]. The IR results revealed that after loading SnO_2, the structure of ATP was well preserved, and the SnO_2 was fully dispersed on ATP surface or framework. The findings are consistent with the XRD results.

The surface acidities of three catalysts including, ATP, 1/4-SnO_2/ATP and 1/2-SnO_2/ATP were measured using NH_3-TPD, and the results are displayed in Fig. 2(c) and Table 1. Generally, based on the desorption temperature of NH_3, temperatures ranging from 50 to 400 °C are classified as weak acid sites, temperatures ranging from 400 to 600 °C are defined as moderate acid sites, and the temperatures>600 °C are categorized as strong acid sites[18]. As shown in Fig. 2(c), three peaks were found for the three catalysts, indicating all three catalysts possess three different strength types of acid sites. Compared with ATP, the strong acid sites of SnO_2/ATP catalysts were increased, while the weak acid sites, medium acid sites and total acid sites were decreased. As summarized in the Table 1, the trend of the strong surface acids is: 1/2-SnO_2/ATP (0.77 mmol/g) > 1/4-SnO_2/ATP (0.74 mmol/g) > ATP (0.56 mmol/g).

Table 1
Acid analysis of catalysts.

Catalysts	Acidity by strength (mmol/g)[a]				Acidity by type[b]		
	weak	moderate	strong	total	B acid (μmol/g)	L acid (μmol/g)	B/L ratio
ATP	0.21	0.74	0.56	1.52	1.97	18.70	0.11
1/4-SnO_2/ATP	0.12	0.30	0.74	1.15	2.85	15.12	0.19
1/2-SnO_2/ATP	0.12	0.28	0.77	1.16	3.83	16.94	0.23

a. Measured using NH_3-TPD. b. Measured using Py-IR.

The types of acid sites (B acid and L acid sites) of catalysts were determined using Py-IR, and the results are shown in and Table 1. The peaks at 1450 and 1610 cm^{-1} could be related to the L acid sites, and the band at 1546 cm^{-1} was associated with the B acid site. The peak at 1490 cm^{-1} indicated that the existence of both the B acid and L acid sites [38]. As can be seen in Fig. 2(d), all three samples presented both B acid and L acid sites. Table 1 summarizes the semi-quantitative concentrations of B acid and L acid sites, and the B/L ratio. The contents of B acid sites and B/L ratio for the three catalysts has the order of: 1/2-SnO_2/ATP > 1/4-SnO_2/ATP > ATP. The findings reveled that after loading SnO_2, the B acid centers of ATP was increased.

Fig. 2(e) gives the N_2 adsorption–desorption isotherms of three different catalysts. Three catalysts exhibited the type IV isotherms and high N_2 uptake with P_0 from 0.4 to 1.0, suggesting that these catalysts have mesoporous and microporous structures. The SnO_2/ATP catalysts presented the similar hysteresis loop types (type H1) with ATP, which indicated that the structure of ATP was well preserved after loading SnO_2. This is also in good agreement with the XRD and FT-IR results. Table 2 tabulates the surface area, pore volume and pore diameter of three catalysts. The total surface area of the SnO_2/ATP catalysts was smaller than that of ATP, demonstrating that SnO_2 partially covered the surface or blocked the channels of ATP. Compared to the ATP, the pore diameter of 1/2-SnO_2/ATP was decreased. However, the pore diameter of 1/4-SnO_2/ATP was increased, which may represent the particle diameter of SnO_2. In addition, the pore structure of the SnO_2/ATP catalyst is further certified by the pore-size distribution curves (Figure S7). The mesoporous surface areas of the three catalysts are ranked in the following order: 1/2-SnO_2/ATP > ATP > 1/4-SnO_2/ATP.

As previously discussed, the catalytic CO_2 desorption activities of the three catalysts were carried out in the following the order: 1/2-SnO_2/ATP > 1/4-SnO_2/ATP > ATP. 1/2-SnO_2/ATP possesses the highest

Table 2
Surface properties of clay catalysts.

Catalysts	surface area (m^2/g)			average pore diameter (nm)	Pore volume (cm^3/g)
	S_{micro}	S_{meso}	S_{BET}		
ATP	32.1	56.8	88.8	7.8	0.13
1/4-SnO_2/ATP	5.5	33.6	39.0	11.0	0.13
1/2-SnO_2/ATP	7.3	69.7	77.0	4.5	0.07

strong acidic sites, B acid sties, and B/L ratio, followed by 1/4-SnO_2/ATP and ATP. Moreover, the highest mesoporous surface area was found in 1/2-SnO_2/ATP. Accordingly, it can be concluded that the strong acid sites, B acid sites and mesoporous surface area of catalyst contribute significantly to enhancing the catalytic activity for CO_2 desorption in rich amine solution. The catalyst contains more B acid sites and larger mesoporous surface area, which can expose more catalytic active sites and provide more protons for carbamates, bicarbonates and carbonates to make them decomposition, thereby desorbing a significant quantity of CO_2 during the rich amine solution regeneration process.

3.4. Confirmation of catalytic effect

FT-IR technique was used to confirm the catalytic CO_2 desorption enhancement effect and provide guidance for investigating the catalytic desorption mechanism over 1/2-SnO_2/ATP. The lean MEA solutions sampled at various times during solvent regeneration with and without 1/2-SnO_2/ATP catalyst were characterized using FT-IR, and the results are shown in Fig. 3. The peaks at 1566, 1490, and 1327 cm^{-1} are assigned to $MEACOO^-$ [49–52]. Here, the peak at 1566 cm^{-1} is related to the asymmetric stretching of COO^-, the peak at 1490 cm^{-1} is associated with the symmetric stretching of COO^-, and the band at 1327 cm^{-1} correlates with the stretching vibration of *N*-COO^-. The bands at 1630 and 1385 cm^{-1} are attributed to the CO_3^{2-} and HCO_3^-[53,54], respectively. As shown in Fig. 3(a), the peak intensities of HCO_3^-, $MEACOO^-$ and CO_3^{2-} for the MEA solution derived from the non-catalytic desorption declined slowly with increasing desorption time. On the other hand, the peak intensities of HCO_3^-, $MEACOO^-$ and CO_3^{2-} decreased much faster in the MEA solution with catalytic regeneration than in the solution without catalytic regeneration, particularly within 15 to 20 min (Fig. 3(b)). The significant catalytic effect of 1/2-SnO_2/ATP was thus verified by the observed alterations in IR peak intensities of intermediate species. The findings indicated that the proton transfer was made easier by using 1/2-SnO_2/ATP catalyst (donating protons), which greatly ameliorated the strong endothermic reaction of $MEACOO^-$ decomposing. Therefore, 1/2-SnO_2/ATP could considerably increase the rate of CO_2 desorption and reduce the regeneration energy requirement.

3.5. Catalytic mechanism

The zwitterion mechanism is commonly accepted to explain the CO_2 desorption process in rich MEA solution. The decomposition of carbamate ($MEACOO^-$) (Eq. (1)) and the deprotonation of protonated amine ($MEAH^+$) (Eqs. (2–3)) are thought to be the two main reactions involved in the regeneration of rich amine solution. $MEACOO^-$ decomposition is mainly determined by the availability of protons, which can be given through $MEAH^+$ deprotonation process. Nevertheless, proton transfer is challenging under basic conditions and low desorption temperatures, and thus demands a lot of energy input. Despite the fact that HCO_3 could accelerate the $MEAH^+$ deprotonation reaction, the amount of HCO_3^- in MEA solution is rather low [55]. Therefore, as a result of the lack of protons and the strong endothermic nature of two reactions (Eqs. (1), (2)), the regeneration of rich amine solution consumes intensive energy.

$$MEA\text{-}COO^- + H_3O \rightleftarrows Zwitterion \rightleftarrows MEA + CO_2\uparrow \quad (1)$$

$$MEAH^+ + H_2O \rightleftarrows MEA + H_3O^+ \quad (2)$$

$$MEAH^+ + HCO_3^- \rightleftarrows MEA + H_2CO_3 \quad (3)$$

As previously evidenced, 1/2-SnO_2/ATP could significantly accelerate the rate of CO_2 desorption and reduce regeneration energy consumption. The possible reason is that the abundant B acid sites (Cat-H) carried by 1/2-SnO_2/ATP donated protons to facilitate the decomposition of $MEACOO^-$, while the conjugate base of B acid sites (Cat^-) can act as temporary proton carriers to quicken the deprotonation of $MEAH^+$. The possible catalytic steps are as follows (Eqs. (4)–(6)).

$$MEA\text{-}COO^- + Cat\text{-}H \rightleftarrows Zwitterion \rightleftarrows MEA + CO_2 + Cat^- \quad (4)$$

$$Cat^- + MEAH^+ \rightleftarrows MEA + Cat\text{-}H \quad (5)$$

$$Cat\text{-}H + H_2O \rightleftarrows Cat^- + H_3O^+ \quad (6)$$

A potential reaction pathway for the SnO_2/ATP catalyzed CO_2 desorption in a rich MEA solution is given in Fig. 4. The conjugate base sites take part in the $MEAH^+$ deprotonation following the introduction of SnO_2/ATP catalyst by bringing protons from $MEAH^+$ to $MEACOO^-$. The protons from the deprotonation reaction or the SnO_2/ATP catalyst react with $MEACOO^-$ to convert it to MEACOOH in the process of $MEACOO^-$ breakdown. After that, O atoms are attacked by L acid sites (unsaturated metal atoms, Sn^{4+}), and a chemisorption process follows. The protons then move from the O atom to the N atom via an isomerization process. After that, the electron lone pairs of N atom are taken away by the acid sites, its configuration is changed from sp2 to sp3, and stretching weakens strength of the C—N bond. The L acid sites also continue to attack the N atoms and aid in stretching the C—N bond, thus increasing the activity of CO_2 desorption. Finally, the zwitterion is split into MEA and CO_2 after the C—N bond is broken. The abundant B acid sites in 1/2-SnO_2/ATP can also provide protons to react with CO_3^{2-} and HCO_3^- to decompose into CO_2 and H_2O. Protons provided by $MEAH^+$ deprotonation can be used to replenish the SnO_2/ATP catalyst.

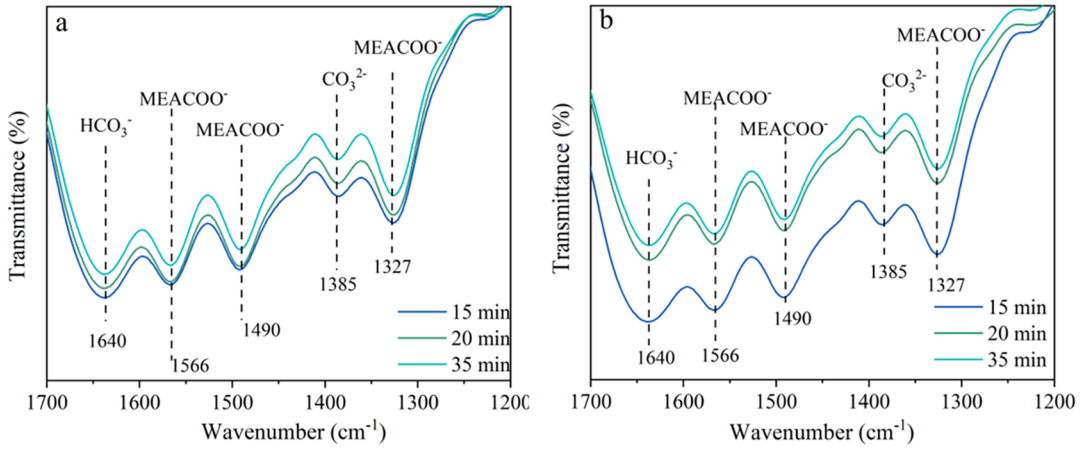

Fig. 3. FT-IR spectra of amine solutions sampled at different times during CO_2 desorption process. (a) MEA solution without catalyst. (b) MEA solution with 1/2-SnO_2/ATP catalyst.

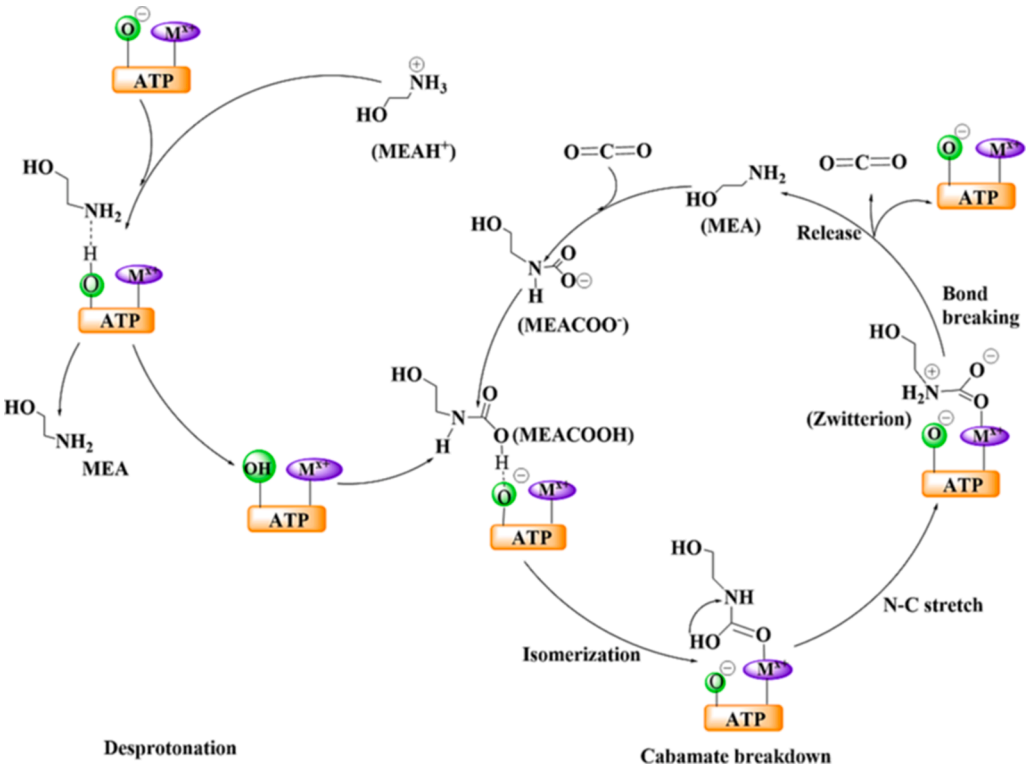

Fig. 4. A possible catalytic CO_2 desorption mechanism over SnO_2/ATP catalyst.

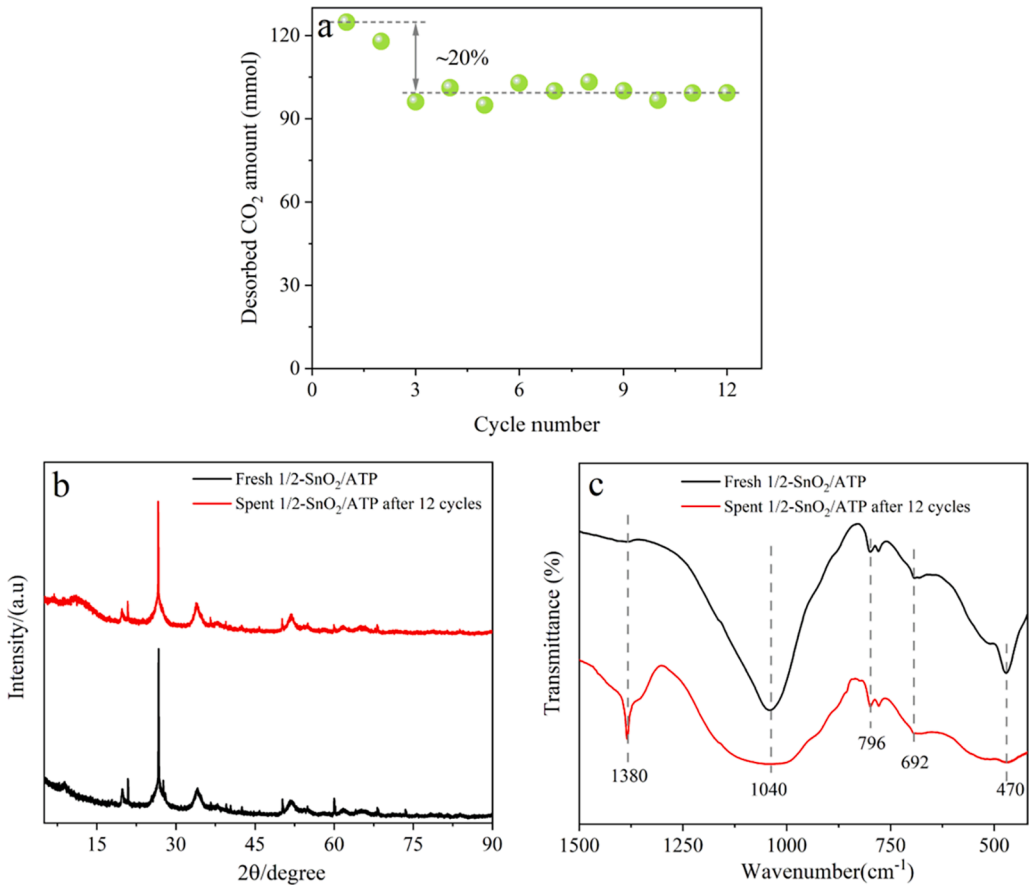

Fig. 5. Cyclic stability test of 1/2-SnO_2/ATP. (a) Catalyzed cyclic CO_2 absorption–desorption by 1/2-SnO_2/ATP. (b) XRD pattern of the spent catalyst after the 12 cycles. (c) FT-IR spectrum of the spent catalyst after the 12 cycles. Absorption conditions, solution: 200 mL 5 M lean MEA solution, absorption gas: containing 50 vol% CO_2 and 50 vol% N_2 at a flow rate of 1000 mL/min, absorption time: 4800 s. Desorption conditions, solution: 200 mL 5 M rich MEA solution with the initial CO_2 loading of 0.545 (±0.01) mol CO_2/mol amine, desorption temperature: 25–88 °C, catalyst dosage: 2.5 g (1.25 wt%), flow rate of N_2: 500 mL/min, desorption time: 4800 s.

3.6. Stability of catalyst

The stability of the solid catalyst is crucial for its industrial application. Twelve CO_2 absorption–desorption cyclic experiments were performed to evaluate the recycling stability of 1/2-SnO_2/ATP catalyst, and the results are shown in Fig. 5 and Figure S6. It is noted that the catalytic activity of 1/2-SnO_2/ATP declined by about 20 % after second cycle and kept essentially unchanged thereafter. The CO_2 desorption quantity for the first cycle was about 124 mmol, and the average CO_2 desorption amount for the following ten cycles was about 99 mmol, which meant that approximately 80 % of the catalytic activity was remained after 12 cycles. The result demonstrated that 1/2-SnO_2/ATP catalyst has excellent cycling stability.

The 1/2-SnO_2/ATP was filtered, washed, dried and then characterized by XRD and FT-IR after 12 cycles of testing. Fig. 5 (b) and (c) indicated that the structure and composition of the spent catalyst did not changed. The new peak appearing at 1380 cm^{-1} in Fig. 5(c) is probably a distorted vibration of $–CH_2$ [56], which may originate from the MEA that has not been fully washed. The outcomes further proved that the stability of 1/2-SnO_2/ATP is excellent, which is helpful for its industrial use.

4. Conclusions

In conclusion, the SnO_2/ATP catalyst possesses the improved B acid sites and strong acid sites, which considerably boosted the CO_2 desorption rate and quantity of CO_2 desorption by 265 % and 222 %, respectively, as compared to blank run. The relative heat duty was effectively reduced by around 52 % compared to the non-catalytic process thanks to the SnO_2/ATP acid catalyst had the ability to lower the energy barrier of CO_2 desorption. SnO_2/ATP also exhibited prominent cyclic stability. The further benefit of the SnO_2/ATP catalyzed-CO_2 desorption is that its maximum temperature can be lower than 100 °C, therefore minimizing the evaporation energy consumption, preventing amine solution degradation, and essentially overcoming the obstacle of intense heat duty for amine solution regeneration. As a result, the SnO_2/ATP catalyst can be regarded as a promising catalyst for facilitating CO_2 desorption and lowering the heat duty for CO_2 capture, and further encouraging the implementation of CCS in real world.

CRediT authorship contribution statement

Zhan Tan: Data curation, Validation, Formal analysis, Writing – original draft. **Shangshang Zhang:** Data curation. **Fangfan Zhao:** Formal analysis. **Rui Zhang:** Formal analysis. **Feiying Tang:** Formal analysis. **Kuiyi You:** Conceptualization, Supervision, Funding acquisition. **He'an Luo:** Supervision. **Xiaowen Zhang:** Supervision, Writing – original draft, Funding acquisition.

Declaration of Competing Interest

The authors declare that they have no known competing financial interests or personal relationships that could have appeared to influence the work reported in this paper.

Data availability

Data will be made available on request.

Acknowledgements

This work was supported by the National Natural Science Foundation of China (22208271), the China Postdoctoral Science Foundation (2021M702746, 2021M692704), Science and Technology Innovation Program of Hunan Province (2021RC2089, 2020RC2074), Guangdong Basic and Applied Basic Research Foundation (2021A1515110136, 2019A1515110919, 2021A1515110789), Natural Science Foundation of Hunan Province (2022JJ40434, 2021JJ40531), Key Research and Development Program in Hunan Province (2019GK2041), Research fund of Hunan Provincial Education Department (21B0166, 20B550), fund of Key Laboratory of Low-grade Energy Utilization Technologies and Systems (LLEUTS-202221), and Training Program of Innovation and Entrepreneurship for Undergraduates of Xiangtan University.

Appendix A. Supplementary data

Supplementary data to this article can be found online at https://doi.org/10.1016/j.cej.2022.139801.

References

[1] M. Bui, C.S. Adjiman, A. Bardow, E.J. Anthony, A. Boston, S. Brown, P.S. Fennell, S. Fuss, A. Galindo, L.A. Hackett, Carbon capture and storage (CCS): the way forward, Energy Environ. Sci. 11 (5) (2018) 1062–1176.
[2] S. Zhang, Y. Shen, L. Wang, J. Chen, Y. Lu, Phase change solvents for post-combustion CO_2 capture: Principle, advances, and challenges, Appl. Energy 239 (2019) 876–897.
[3] X. Ye, Y. Lu, CO_2 absorption into catalyzed potassium carbonate–bicarbonate solutions: Kinetics and stability of the enzyme carbonic anhydrase as a biocatalyst, Chem. Eng. Sci. 116 (2014) 567–575.
[4] G. Hu, N.J. Nicholas, K.H. Smith, K.A. Mumford, S.E. Kentish, G.W. Stevens, Carbon dioxide absorption into promoted potassium carbonate solutions: A review, Int. J. Greenhouse Gas Control 53 (2016) 28–40.
[5] G.T. Rochelle, Amine scrubbing for CO_2 capture, Science 325 (5948) (2009) 1652–1654.
[6] X. Zhang, Y. Huang, H. Gao, X. Luo, Z. Liang, P. Tontiwachwuthikul, Zeolite catalyst-aided tri-solvent blend amine regeneration: An alternative pathway to reduce the energy consumption in amine-based CO_2 capture process, Appl. Energy 240 (2019) 827–841.
[7] R. Zhang, X. He, T. Liu, C.e. Li, M. Xiao, H. Ling, X. Hu, X. Zhang, F. Tang, H.a. Luo, Thermodynamic studies for improving the prediction of CO_2 equilibrium solubility in aqueous 2-dimethylamino-2-methyl-1-propanol, Separation Purification Technology 295 (2022) 121292.
[8] R. Zhang, T. Li, Y. Zhang, J. Ha, Y. Xiao, C.e. Li, X. Zhang, H.a. Luo, CuO modified KIT-6 as a high-efficiency catalyst for energy-efficient amine solvent regeneration, Separation Purification Technology 300 (2022) 121702.
[9] F. de Meyer, C. Bignaud, The use of catalysis for faster CO_2 absorption and energy-efficient solvent regeneration: An industry-focused critical review, Chem. Eng. J. 428 (2022), 131264.
[10] Z. Liang, W. Rongwong, H. Liu, K. Fu, H. Gao, F. Cao, R. Zhang, T. Sema, A. Henni, K. Sumon, Recent progress and new developments in post-combustion carbon-capture technology with amine based solvents, Int. J. Greenhouse Gas Control 40 (2015) 26–54.
[11] X. Zhang, R. Zhang, H. Liu, H. Gao, Z. Liang, Evaluating CO_2 desorption performance in CO_2-loaded aqueous tri-solvent blend amines with and without solid acid catalysts, Appl. Energy 218 (2018) 417–429.
[12] S. Zhang, M. Du, P. Shao, L. Wang, J. Ye, J. Chen, J. Chen, Carbonic anhydrase enzyme-MOFs composite with a superior catalytic performance to promote CO_2 absorption into tertiary amine solution, Environ. Sci. Technol. 52 (21) (2018) 12708–12716.
[13] K. Li, P. van der Poel, W. Conway, K. Jiang, G. Puxty, H. Yu, P. Feron, Mechanism investigation of advanced metal-ion-mediated amine regeneration: a novel pathway to reducing CO_2 reaction enthalpy in amine-based CO_2 capture, Environ. Sci. Technol. 52 (24) (2018) 14538–14546.
[14] B. Feng, M. Du, T.J. Dennis, K. Anthony, M.J. Perumal, Reduction of energy requirement of CO_2 desorption by adding acid into CO_2-loaded solvent, Energy Fuels 24 (1) (2009) 213–219.
[15] Z. Zhang, J. Cai, F. Chen, H. Li, W. Zhang, W. Qi, Progress in enhancement of CO_2 absorption by nanofluids: A mini review of mechanisms and current status, Renewable Energy 118 (2018) 527–535.
[16] D. Nguyen, J. Stolaroff, A. Esser-Kahn, Solvent effects on the photothermal regeneration of CO_2 in monoethanolamine nanofluids, ACS Appl. Mater. Interfaces 7 (46) (2015) 25851–25856.
[17] X. Zhang, H. Liu, Z. Liang, R. Idem, P. Tontiwachwuthikul, M.J. Al-Marri, A. Benamor, Reducing energy consumption of CO_2 desorption in CO_2-loaded aqueous amine solution using Al_2O_3/HZSM-5 bifunctional catalysts, Appl. Energy 229 (2018) 562–576.
[18] U.H. Bhatti, A.K. Shah, A. Hussain, H.A. Khan, C.Y. Park, S.C. Nam, I.H. Baek, Catalytic activity of facilely synthesized mesoporous HZSM-5 catalysts for optimizing the CO_2 desorption rate from CO_2-rich amine solutions, Chem. Eng. J. 389 (2020), 123439.
[19] L. Xing, K. Wei, Y. Li, Z. Fang, Q. Li, T. Qi, S. An, S. Zhang, L. Wang, TiO_2 Coating Strategy for Robust Catalysis of the Metal-Organic Framework toward Energy-Efficient CO_2 Capture, Environmental Science Technology 55 (16) (2021) 11216–11224.
[20] M.S. Alivand, O. Mazaheri, Y. Wu, A. Zavabeti, A.J. Christofferson, N. Meftahi, S. P. Russo, G.W. Stevens, C.A. Scholes, K.A. Mumford, Engineered assembly of water-

dispersible nanocatalysts enables low-cost and green CO_2 capture, Nat. Commun. 13 (1) (2022) 1–11.
[21] Q. Lai, S. Toan, M.A. Assiri, H. Cheng, A.G. Russell, H. Adidharma, M. Radosz, M. Fan, Catalyst-TiO $(OH)_2$ could drastically reduce the energy consumption of CO_2 capture, Nat. Commun. 9 (1) (2018) 1–7.
[22] X. Zhang, Y. Huang, J. Yang, H. Gao, Y. Huang, X. Luo, Z. Liang, P. Tontiwachwuthikul, Amine-based CO_2 capture aided by acid-basic bifunctional catalyst: Advancement of amine regeneration using metal modified MCM-41, Chem. Eng. J. 383 (2020), 123077.
[23] X. Zhang, Z. Zhu, X. Sun, J. Yang, H. Gao, Y. Huang, X. Luo, Z. Liang, P. Tontiwachwuthikul, Reducing energy penalty of CO_2 capture using Fe promoted SO_4^{2-}/ZrO_2/MCM-41 catalyst, Environmental science technology 53 (10) (2019) 6094–6102.
[24] X. Zhang, J. Hong, H. Liu, X. Luo, W. Olson, P. Tontiwachwuthikul, Z. Liang, SO_4^{2-}/ZrO_2 supported on γ-Al_2O_3 as a catalyst for CO_2 desorption from CO_2-loaded monoethanolamine solutions, AIChE J. 64 (11) (2018) 3988–4001.
[25] X. Zhang, X. Zhang, H. Liu, W. Li, M. Xiao, H. Gao, Z. Liang, Reduction of energy requirement of CO_2 desorption from a rich CO_2-loaded MEA solution by using solid acid catalysts, Appl. Energy 202 (2017) 673–684.
[26] Q. Sun, H. Gao, Y. Mao, T. Sema, S. Liu, Z. Liang, Efficient nickel-based catalysts for amine regeneration of CO_2 capture: From experimental to calculations verifications, AIChE J. (2021) e17706.
[27] L. Xing, K. Wei, Q. Li, R. Wang, S. Zhang, L. Wang, One-Step Synthesized SO_4^{2-}/ZrO_2-HZSM-5 Solid Acid Catalyst for Carbamate Decomposition in CO_2 Capture, Environmental Science Technology 54 (21) (2020) 13944–13952.
[28] Y. Li, Z. Chen, G. Zhan, B. Yuan, L. Wang, J. Li, Inducing efficient proton transfer through Fe/Ni@ COF to promote amine-based solvent regeneration for achieving low-cost capture of CO_2 from industrial flue gas, Separation Purification Technology 298 (2022), 121676.
[29] K. Wei, L. Xing, Y. Li, T. Xu, Q. Li, L. Wang, Heteropolyacid Modified Cerium-based MOFs Catalyst for Amine Solution Regeneration in CO_2 Capture, Separation Purification Technology 293 (2022), 121144.
[30] U.H. Bhatti, D. Sivanesan, D.H. Lim, S.C. Nam, S. Park, I.H. Baek, Metal oxide catalyst-aided solvent regeneration: A promising method to economize post-combustion CO_2 capture process, J. Taiwan Inst. Chem. Eng. 93 (2018) 150–157.
[31] U.H. Bhatti, S. Nam, S. Park, I.H. Baek, Performance and mechanism of metal oxide catalyst-aided amine solvent regeneration, ACS Sustainable Chem. Eng. 6 (9) (2018) 12079–12087.
[32] Y.M. Sani, W.M.A.W. Daud, A.A. Aziz, Activity of solid acid catalysts for biodiesel production: a critical review, Appl. Catal. A 470 (2014) 140–161.
[33] X.-Y. Li, Y. Jiang, X.-Q. Liu, L.-Y. Shi, D.-Y. Zhang, L.-B. Sun, Direct synthesis of zeolites from a natural clay, attapulgite, ACS Sustainable Chemistry Engineering 5 (7) (2017) 6124–6130.
[34] M. Cui, P. Mu, Y. Shen, G. Zhu, L. Luo, J. Li, Three-dimensional attapulgite with sandwich-like architecture used for multifunctional water remediation, Separation Purification Technology 235 (2020), 116210.
[35] B. Yuan, X.-Q. Yin, X.-Q. Liu, X.-Y. Li, L.-B. Sun, Enhanced hydrothermal stability and catalytic performance of HKUST-1 by incorporating carboxyl-functionalized attapulgite, ACS Applied Materials Interfaces 8 (25) (2016) 16457–16464.
[36] A.M. Awad, R.S. Shifa M., R. Jalab, M. H.Gulied, M. S.Nasser, A. Benamor, S. Adham, Adsorption of organic pollutants by natural and modified clays: A comprehensive review, Separation Purification Technology (228) (2019) 115719.
[37] X.-Y. Li, D.-Y. Zhang, X.-Q. Liu, L.-Y. Shi, L.-B. Sun, A tandem demetalization–desilication strategy to enhance the porosity of attapulgite for adsorption and catalysis, Chem. Eng. Sci. 141 (2016) 184–194.
[38] Z. Tan, S. Zhang, X. Yue, F. Zhao, F. Xi, D. Yan, H. Ling, R. Zhang, F. Tang, K. You, H.a. Luo, X. Zhang, Attapulgite as a cost-effective catalyst for low-energy consumption amine-based CO_2 capture, Separation and Purification Technology 298 (2022).
[39] Y. Wang, C. Wang, M. Chen, Z. Tang, Z. Yang, J. Hu, H. Zhang, Hydrogen production from steam reforming ethanol over Ni/attapulgite catalysts-Part I: effect of nickel content, Fuel Process. Technol. 192 (2019) 227–238.
[40] W. Wang, A. Wang, Recent progress in dispersion of palygorskite crystal bundles for nanocomposites, Appl. Clay Sci. 119 (2016) 18–30.
[41] X. Zhou, X. Huang, A. Xie, S. Luo, C. Yao, X. Li, S. Zuo, V_2O_5-decorated Mn-Fe/attapulgite catalyst with high SO_2 tolerance for SCR of NO_x with NH_3 at low temperature, Chem. Eng. J. 326 (2017) 1074–1085.
[42] Y. Wang, M. Chen, X. Li, Z. Yang, T. Liang, Z. Zhou, Y. Cao, Hydrogen production via steam reforming of ethylene glycol over Attapulgite supported nickel catalysts, Int. J. Hydrogen Energy 43 (45) (2018) 20438–20450.
[43] B. Mallesham, A. Rangaswamy, B.G. Rao, T.V. Rao, B.M. Reddy, Solvent-Free Production of Glycerol Carbonate from Bioglycerol with Urea Over Nanostructured Promoted SnO_2 Catalysts, Catal. Lett. 150 (12) (2020).
[44] B. Mallesham, P. Sudarsanam, B.M. Reddy, Production of biofuel additives from esterification and acetalization of bioglycerol over SnO_2-based solid acids, Industrial Engineering Chemistry Research 53 (49) (2014) 18775–18785.
[45] J.N. Heda, P.S. Niphadkar, V.V. Bokade, Efficient Synergetic Combination of H-USY and SnO_2 for Direct Conversion of Glucose into Ethyl Levulinate (Biofuel Additive), Energy Fuels 33 (3) (2019) 2319–2327.
[46] H. Tian, Y. Shao, C. Liang, Q. Xu, L. Zhang, S. Zhang, S. Liu, X. Hu, Sulfated attapulgite for catalyzing the conversion of furfuryl alcohol to ethyl levulinate: Impacts of sulfonation on structural transformation and evolution of acidic sites on the catalyst, Renewable Energy 162 (2020) 1576–1586.
[47] B.J. Wang, S.Y. Ma, S.T. Pei, X.L. Xu, P.F. Cao, J.L. Zhang, R. Zhang, X.H. Xu, T. Han, High specific surface area SnO_2 prepared by calcining Sn-MOFs and their formaldehyde-sensing characteristics, Sens. Actuators, B 321 (2020).
[48] B. Tyagi, C.D. Chudasama, R.V. Jasra, Determination of structural modification in acid activated montmorillonite clay by FT-IR spectroscopy, Spectrochim Acta A Mol Biomol Spectrosc 64 (2) (2006) 273–278.
[49] J.-B. Bossa, F. Borget, F. Duvernay, P. Theulé, T. Chiavassa, Formation of neutral methylcarbamic acid ($CH_3NHCOOH$) and methylammonium methylcarbamate [CH_3NH^{3+}][CH_3NHCO^{2-}] at low temperature, The Journal of Physical Chemistry A 112 (23) (2008) 5113–5120.
[50] S.E. Cabaniss, I.F. McVey, Aqueous infrared carboxylate absorbances: aliphatic monocarboxylates, Spectrochim. Acta Part A Mol. Biomol. Spectrosc. 51 (13) (1995) 2385–2395.
[51] P. Jackson, K. Robinson, G. Puxty, M. Attalla, In situ Fourier Transform-Infrared (FT-IR) analysis of carbon dioxide absorption and desorption in amine solutions, Energy Procedia 1 (1) (2009) 985–994.
[52] K. Robinson, A. McCluskey, M.I. Attalla, An FTIR spectroscopic study on the effect of molecular structural variations on the CO_2 absorption characteristics of heterocyclic amines, ChemPhysChem 12 (6) (2011) 1088–1099.
[53] M. Falk, A.G. Miller, Infrared spectrum of carbon dioxide in aqueous solution, Vib. Spectrosc. 4 (1) (1992) 105–108.
[54] G. Richner, G. Puxty, Assessing the Chemical Speciation during CO_2 Absorption by Aqueous Amines Using in Situ FTIR, Ind. Eng. Chem. Res. 51 (44) (2012) 14317–14324.
[55] H. Liu, X. Zhang, H. Gao, Z. Liang, R. Idem, P. Tontiwachwuthikul, Investigation of CO_2 Regeneration in Single and Blended Amine Solvents with and without Catalyst, Ind. Eng. Chem. Res. 56 (27) (2017) 7656–7664.
[56] Y.S. Mary, C.Y. Panicker, H.T. Varghese, C. Van Alsenoy, M. Procházková, R. Ševčík, P. Pazdera, Acid-base properties, FT-IR, FT-Raman spectroscopy and computational study of 1-(pyrid-4-yl) piperazine, Spectrochim. Acta Part A Mol. Biomol. Spectrosc. 121 (2014) 436–444.